

Directivity in RF Sensor Networks for Widespread Spectrum Monitoring

Nikolaus Kleber, *Member, IEEE*, Martin Haenggi, *Fellow, IEEE*, Jonathan Chisum, *Senior Member, IEEE*, Bertrand Hochwald, *Fellow, IEEE*, J. Nicholas Laneman, *Fellow, IEEE*

Abstract—Widespread RF spectrum monitoring could enable data-driven modeling of spectrum usage, enhance spectral utilization, and help automate policy enforcement. Previous works in wireless sensor networks offer design insights for RF sensors, but they assume emitters that radiate omnidirectionally. This paper develops a new framework for directional sensors and emitters, which are increasingly common with the growth of millimeter wave technologies. We focus on two-dimensional random sensor deployments modeled as Poisson point processes. Specifically, we determine the probability that a sensor network detects a single emitter for a channel model including path loss, fading, and the directivity of emitters and sensors with random orientations and locations. Our results suggest that with a path loss exponent of 4, quartering the emitter half-power beamwidth doubles the required average sensor density. We also conclude that omnidirectional sensors optimize detection probability. For multiple emitters, we develop a lower bound on the probability of multi-emitter detection and find the average number of undetected emitters. Finally, assuming higher sensor quality results in higher sensor cost, we consider a fixed-budget deployment and observe that decreasing the individual sensor cost by a decade and therefore increasing the quantity of sensors reduces the missed detection probability by about a decade.

Index Terms—Directive antennas, radio spectrum management, cooperative spectrum sensing

I. INTRODUCTION

A. Background

EVEN though the demand of wireless traffic increases, the supply of RF spectrum remains fixed. As a result, usable spectrum has become a scarce resource of increasing value [1], [2]. Solutions are to increase the amount of usable spectrum and/or to use the current spectrum more efficiently. Efforts to expand the usable spectrum are underway with commercial millimeter-wave (mm-wave) technology (see [3] and references therein). Here we focus on more efficient utilization of the widely-used sub-6 GHz spectrum, but strategies for efficiency apply beyond 6 GHz. Regulatory institutions currently rely on theoretical models of limited accuracy and unverified claims by licensees to determine spectrum usage

This work was supported by the U.S. National Science Foundation (NSF) under grant IIP 14-39682, joint funding by NSF and Intel under grant ECCS-2002921, and partial support by the Army Research Laboratory accomplished under grant W911NF-16-2-0140.

N. Kleber was with the Department of Electrical Engineering, University of Notre Dame, Notre Dame, IN 46556 USA. He is now with Raytheon Technologies RIS, Fort Wayne, IN 46808 USA.

M. Haenggi, J. Chisum, B. Hochwald, and J.N. Laneman are with the Department of Electrical Engineering at the University of Notre Dame, Notre Dame, IN 46556 USA; e-mail: {mhaenggi, jchisum, bhochwal, jnl}@nd.edu.

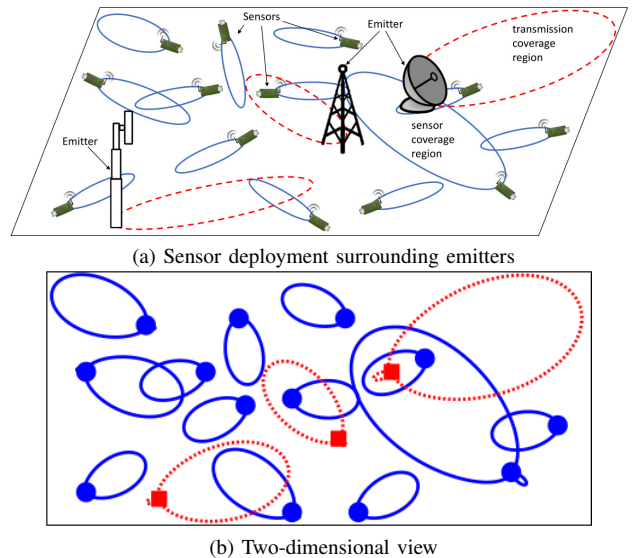


Fig. 1. Illustration of widespread spectrum monitoring system. (a) Randomly deployed sensors measure RF transmissions across a wide spectrum over a wide geographical area. Emitters with various operating frequencies, locations, and antennas can be detected. (b) Two-dimensional view of system highlighting the varying antenna patterns and resulting coverage. Sensor locations and gain patterns are denoted with a blue ‘o’ and solid line, respectively. Emitter locations and gain patterns are denoted with a red square and dotted line, respectively.

and efficiency. The result is underutilized spectrum in some bands [1], [4].

Spectrum monitoring (SM) takes measurements of the spectrum across frequency, time, and space, as illustrated in Fig. 1. If widespread, SM could provide the “ground truth” of spectrum usage and thereby “close the feedback loop” for spectrum management [5]. In particular, SM could provide a wealth of data for data-driven modeling of RF environments [6], which could overcome the limited accuracy of current theoretical models. SM could also provide a data-driven approach to find unoccupied spectrum and inform a spectrum management mechanism (e.g., a spectrum access system (SAS) [7]–[9] with an environmental sensing capability (ESC) [10]) to access it. Additionally, SM could help automate spectrum enforcement [11], which could significantly strengthen and expedite spectrum policy.

Elements of SM have been pursued in a variety of forms over the past decade, including cognitive radios [12], [13], radio environment maps [14], dedicated sensor networks [15], and crowdsourcing [6], [16]–[20]. However, each has experienced economic and/or regulatory roadblocks. From previous

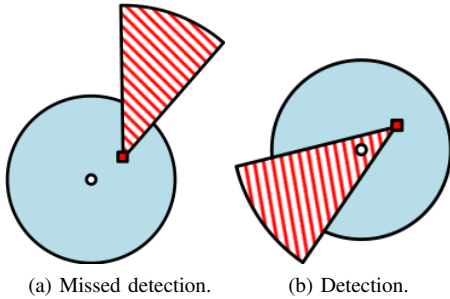


Fig. 2. Example of an omnidirectional sensor (white ‘o’) attempting to detect a directional emitter (red square). In (a) the sensor fails despite the emitter residing in the sensor’s coverage region because the emission is directed away from the sensor. In (b) the sensor succeeds since the emitter radiates toward the sensor.

works, we observe that the prospects of spectrum sharing have improved from TV white space in the 700 MHz band to the Citizens Broadband Radio Service (CBRS) in the 3.5 GHz band. With established standards for sensor data formats [21], coexistence [22], and interoperability [23], we anticipate that opportunities will continue to extend to other frequency bands with time. Moreover, we see from previous works that the widespread deployment of enough spectrum sensors is a crucial problem for SM to be beneficial.

The literature on wireless sensor networks (WSN) has considered the problem of deploying enough sensors to detect emitters, and SM designs can leverage these results. However, several important issues in RF have not been considered in the context of WSN, including directivity of RF emitters, which are common in RF due to significant signal attenuation over large distances and/or at high frequencies [24, Ch. 2]. Unfortunately, previous works on WSN assume the emitters radiate omnidirectionally. To the extent that directionality has been considered, the focus has only been on directional sensors, such as optical, ultrasound, and infrared sensors (*e.g.*, [25] and sources therein). Directional transmission also appears on the sensor side in the context of WSN communication [26]–[28] and secure sensor localization [29].

As illustrated in Fig. 2, if the emitters are directional, an emitter could reside in the typically-assumed omnidirectional coverage region of a sensor yet remain undetected because the emitter’s signal is directed away from the sensor. This problem affects multiple studies [30], [31]. For example, directional emitters undermine the well-known Boolean model [32]. The same problem exists in other design approaches, such as for coverage enhancement algorithms [30], [33]. Consequently, a need exists for a framework that considers directional emitters along with directional sensors.

B. Contributions

This paper considers scenarios in which the deployment is achieved via crowdsourcing (*e.g.*, re-using cell phones as sensors in a commercial context) or simply dropping sensors out of a plane (in a defense context), and are well-modeled by a random deployment of sensors. Demand on sensor resources needs to be low, and while backhaul is assumed to be in place for the sensors, a low required backhaul is desirable

to prevent disruption to the user in the commercial context (*e.g.*, WiFi and LTE) and to satisfy tactical constraints in defense contexts. Consequently, we focus on the application of power detection of emitters to reduce device processing, power consumption, and backhaul traffic. In particular, the sensors return a time-averaged power measurement for a certain center frequency (with some bandwidth). Despite the simplicity of power detection, the information is nonetheless useful for applications such as identifying unused spectrum or bad actors within a region. Other scenarios and applications are of interest but are outside the scope of this paper.

In this paper, we create a general framework to model directional (and omnidirectional) sensors and emitters within a sensor network for SM. The framework supports three dimensions, but this paper focuses on the two-dimensional case. This work addresses the problem of designing a SM system with the aim of power detection in the presence of directional emitters. We focus on the effects of sensor and emitter locations and orientations. For the case when the sensors form a Poisson point process (PPP), we provide a fundamental and general analytic result on the probability that an emitter is detected. The result incorporates all sources of randomness, including channel fading, shadowing, and/or randomly-oriented directional antennas. We also analytically lower bound this probability for multiple emitters of a given number, and we find a closed-form expression for the expected number of undetected emitters within a finite region. We use these analyses to conclude four main points. First, we find an expression to quantify the increase in deployment density of sensors with increasing emitter directivity. Our results suggest that with a path loss exponent of 4 and all other things equal, quartering the emitter half-power beamwidth doubles the average number of sensors needed for detection. Second, we analytically determine optimal sensor characteristics; in particular, we find omnidirectional sensors optimize the probability of detection, regardless of emitter directivity. Third, we analyze the detection probability’s sensitivity to frequency and develop a deployment strategy for multiple frequency bands. Finally, under the constraint of a fixed-budget deployment, we illustrate that sensor quantity improves the system probability of detection more than sensor quality. In particular, from a survey of current software-defined radios, for a given total cost, we observe that decreasing the individual sensor cost by a factor of 10 reduces the system probability of missed detection by about a factor of 10.

C. Related Works

Previous works have taken a similar approach as this paper to model sensor networks. The works in [34]–[37] also model sensors deployments as PPPs with simple path loss channel models for omnidirectional sensors and emitters. The focus of [34] is to find the necessary sensor density based on a Cramér-Rao bound on emitter localization error, whereas our work uses detection probability as the metric. Source detection is similarly the focus of [35]–[37], though with slight variations such as time-constraints for sensor communication [35], the use of estimated likelihood ratios for detection [36], and the

effects of sensor clustering [37]. Our work differs by using power detection based on a more complex channel model that includes fading and directional (sensor and emitter) antennas with random orientations.

Directional sensors with random orientations and locations modeled by a PPP have been considered in [38]. While our work has a similar theme in the model, [38] finds the critical density for sensor coverage and network connectivity percolation for video sensors (with presumed omnidirectionally visual targets). In contrast, we focus on the RF domain with directional emitters and find the required sensor density for a given detection probability rather than percolation.

D. Outline

The remainder of this paper is organized as follows. Sec. II introduces a general framework to model an RF sensor network with directional emitters and sensors and formulates the problems of interest in two dimensions. Sec. III provides the probability of single emitter detection along with several applications. Sec. IV presents results for multiple emitters, including a lower-bound on the probability of multi-emitter detection and the expected number of undetected emitters. Finally, Sec. V provides closing remarks and future directions.

II. SYSTEM MODEL

We now present a general framework to model RF sensor networks and the target emitters, which extends to any number of dimensions d , though the obvious cases of interest are $d = 2$ and 3 dimensions. We focus on cases in which the sensor deployment is well modeled as uniformly random. As illustrated in Fig. 1, we need to describe system parameters of sensor and emitter locations, directionality, and capabilities.

To describe directional sensors, we follow a convention similar to that in [25], though tailored to RF applications. In summary, we characterize a directional sensor deployed in a d -dimensional space with the following pieces of information, which we describe in more detail later:

- the sensor location, denoted $\mathbf{x}^s \in \mathbb{R}^d$,
- the sensor orientation, denoted by an orthonormal rotation matrix $R^s \in \mathbb{R}^{d \times d}$,
- the sensor antenna gain pattern, denoted by the positive function g^s ,
- the sensor sensitivity, described by the minimum detectable signal (MDS) power $\tau^s > 0$.

Similarly, we characterize a directional emitter in a d -dimensional space with

- the emitter location, denoted $\mathbf{x}^e \in \mathbb{R}^d$,
- the emitter orientation, denoted by an orthonormal rotation matrix $R^e \in \mathbb{R}^{d \times d}$,
- the emitter antenna gain pattern, denoted by the positive function g^e ,
- the emitter transmit power, denoted $p^e \geq 0$.

The superscripts s and e denote the value for a sensor or emitter, respectively. If there are n^s sensors and n^e emitters, we use the subscripts $j \in \{1, \dots, n^s\}$ and $i \in \{1, \dots, n^e\}$ to denote the index of the sensor and emitter, respectively. In

TABLE I
NOTATION

Variable, (emitter i , sensor j)	Description	Variable (emitter i , sensor j)	Description
d	dimension	\mathbf{t}	target location
$\mathbf{x}, \mathbf{x}_i^e, \mathbf{x}_j^s$	location	\mathbf{p}	self-location
R, R_i^e, R_j^s	orientation	ϕ	azimuth variable
g, g_i^e, g_j^s	gain function	o	location of origin
$p, p_i^e, p_j^s, p_{ij}^s$	(Tx/Rx) power	$w(n)$	random noise samples
τ, τ_j^s	sensitivity (MDS)	K	number of noise samples
n, n^e, n^s	number (of emitters/sensors)	Z	random noise power
$\mathbf{d}, \mathbf{d}_j^s$	measured data	\mathcal{R}	finite region
Φ, Φ^s	PPP of locations	$\mathcal{E}, \mathcal{E}_i$	detection event
$\lambda, \lambda^e, \lambda^s$	deployment density	\mathcal{D}	all emitters detected event
ψ, ψ_i^e, ψ_j^s	azimuth orientation	N	# of sensors with $p_{ij}^s \geq \tau^s$
α	path loss exponent	$M_{\mathbf{x}}$	mark (random variable) at \mathbf{x}
h, h_{ij}	fading coefficient	δ	$2/\alpha$
κ	path loss model constant	θ	arbitrary threshold
f	frequency	F	CCDF
r_0	reference distance	$b_{\mathbf{x}}$	Bernoulli random variable at \mathbf{x}
c	speed of light	$\Gamma(x)$	gamma function
Ψ, Ψ_i^e, Ψ_j^s	azimuth HPBW	N_0	noise floor
$\Theta, \Theta_i^e, \Theta_j^s$	elevation HPBW	ν	noise figure
η, η^e, η^s	angle fraction	SNR_{out}	application SNR
P_D	detection rate	B	bandwidth
P_F	false alarm rate	T	temperature
C	received power ratio	k_B	Boltzmann constant
ω	power-to-sensitivity ratio	n^u	number missed emitters

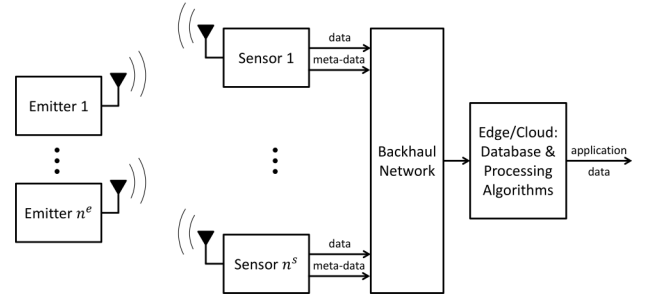


Fig. 3. A high-level block diagram of all the system components and parameters.

other words, we fully describe the j th sensor with the 4-tuple $(\mathbf{x}_j^s, R_j^s, g_j^s, \tau_j^s)$, and we describe the i th emitter with the 4-tuple $(\mathbf{x}_i^e, R_i^e, g_i^e, p_i^e)$. A summary of the notation used in this paper is in Table I.

We now briefly describe the system architecture. A diagram of n^s sensors and n^e emitters is given in Fig. 3. Generally, we collect all sensor data in a centralized database for processing. Each sensor can determine its location \mathbf{x}_j^s via a mechanism, such as GPS, WiFi, or LTE positioning. Similarly, each sensor can determine its orientation R_j^s via a compass or accelerometer. The sensor gain g_j^s and sensitivity τ_j^s are inherent to the device and can be recorded in the sensor software before

deployment. The data sent over the backhaul to the database includes the sensor characteristics $(\mathbf{x}_j^s, R_j^s, g_j^s, \tau_j^s)$ and the collected data, \mathbf{d}_j^s , for $j \in \{1, \dots, n^s\}$. The sensor data can be used toward several ends, such as estimating the number of emitters, the emitter locations, the emitter orientations, and/or the emitter transmission powers [39]. However, estimating emitter parameters is outside the scope of this paper.

A. Random Deployment

In our scenario of interest, the sensor deployment is well modeled as random in location and orientation. This model is reasonable because we have no prior knowledge of sensor locations nor their orientations. Emitters are arbitrarily located with random orientations, as well.

1) *Locations*: We describe location with a vector $\mathbf{x} \in \mathbb{R}^d$ representing Cartesian coordinates. In general, the locations of a random deployment of sensors are well modeled by a PPP, denoted Φ^s , with location-dependent density $\lambda^s(\mathbf{x})$ [32]. Mathematically, $\Phi^s = (\mathbf{x}_j^s)_{j \in \mathbb{N}}$. From a $d = 2$ dimensional perspective, the deployment is well modeled as uniformly random, which implies a homogeneous density, $\lambda^s(\mathbf{x}) \equiv \lambda^s$. If $d > 2$, the deployment may no longer be uniformly random in all dimensions, but a PPP with an inhomogeneous density $\lambda^s(\mathbf{x})$ can be used. Note if we condition on the number of locations in a finite region of interest, the locations are iid uniform in the region, forming a binomial point process (BPP).

For the case of a single emitter, the detection probability does not depend on the emitter's location since the PPP is stationary [32, Sec. 2.6]. For convenience, we state that the emitter is at the origin.

2) *Orientations*: Describing the orientation of an antenna can be achieved in several ways. We define the orientation of the sensor antenna via a rotation from a given default orientation. In particular, we define the rotation with an orthogonal rotation matrix R , which is a product of Givens rotations.¹ Generally, we set the convention that the main lobe of the antenna gain pattern lies along an axis of the coordinate system.

For the two-dimensional case, the rotation matrix is

$$R = \begin{bmatrix} \cos \psi & -\sin \psi \\ \sin \psi & \cos \psi \end{bmatrix}, \quad (1)$$

where ψ indicates the direction of the main lobe. In the scenario of a random deployment, the orientations of the sensors and emitters are iid uniformly distributed, which means R_j^s and R_i^e are iid uniform rotations. Note that uniformly random rotations translates into ψ_j^s and ψ_i^e being iid uniform on $[0, 2\pi)$.

B. Sensor and Emitter Capabilities

For simplicity, we consider the case in which the sensors are deployed with the same antennas that share a common gain pattern ($g_j^s(\cdot) \equiv g^s(\cdot) \forall j$). Similarly, all emitters share

the same gain pattern $g^e(\cdot)$, which is known. This scenario is reasonable because emitters operating in the same frequency range likely have similar antennas, and we would prepare the sensors in an identical fashion with antennas that operate in the same frequency range as the emitters. Usually, publicly available regulations limit the transmission power of emitters, and often emitters transmit at the legal maximum to obtain the highest SNR possible, so we can say that all emitter powers are equal and known ($p_i^e \equiv p^e \forall i$). Similarly, it is reasonable to say that the sensors are constructed to be approximately the same, so all sensors have the same sensitivity ($\tau_j^s \equiv \tau^s \forall j$).

Finally, we consider scenarios in which there are discernible differences among the emitter signals and power levels across time, frequency, spreading codes, and/or high-level protocols. For example, a spectrogram of multiple stationary emitters following the LTE standard could illustrate varying power levels across time and frequency due to different separation distances from the emitters to the sensor. A distribution of the different power levels from the spectrogram could reveal distinct patterns, each of which would identify a particular emitter. Certain signaling structures could be exploited as well, e.g., primary and secondary synchronization signals (PSS and SSS) in LTE or clear channel assessment (CCA) in WiFi. Furthermore, a wide body of machine learning techniques can be applied to distinguish emitters based on modulation scheme [40], MAC protocol [41], and communication technology [12]. In particular, clustering of selected features can distinguish spatially separated emitters, even with the same system characteristics [42], [43]. As a result, the sensors should be able to separate the individual emitter signals through low-level signal processing and calculate distinct power measurements for each emitter. In particular, for this paper we are interested in the sensor calculations of p_{ij}^s , the time-averaged received power from the i th emitter measured at the j th sensor. In practice, the sensors provide estimates \widehat{p}_{ij}^s along with an estimate of the noise floor \widehat{N}_0 , which could differ from the exact p_{ij}^s and N_0 . We address this issue in a later section.

1) *Sensor Sensitivity*: The sensor sensitivity is determined by several factors [44]. First, let τ^s denote the power of the minimum detectable signal by the sensor. Let the equivalent noise figure (ν) of the entire RF chain in the receiver be given by

$$\nu = \frac{\text{SNR}_{\text{in}}}{\text{SNR}_{\text{out}}} = \frac{S_{\text{in}}/N_{\text{in}}}{S_{\text{out}}/N_{\text{out}}}. \quad (2)$$

Rearranging the terms to solve for the signal power into the device yields

$$S_{\text{in}} = \nu(S_{\text{out}}/N_{\text{out}})N_{\text{in}}. \quad (3)$$

Based on our application, the sensor will have a required minimum SNR_{out} to perform its task properly. The noise figure is inherent to the device, and the input noise is assumed to be thermal noise given by $N_{\text{in}} = k_B T B$, where B is the bandwidth of the system, T is the temperature (in Kelvin) of the system, and k_B is the Boltzmann constant [45]. If the noise figure ν and minimum SNR_{out} for the receiver are known, S_{in} in (3) gives the power of the minimum detectable signal

¹A Givens rotation only occurs within one plane. Consequently, to achieve rotation in more than two dimensions, multiple Givens rotations in different planes must occur. Consistent with matrix multiplication, the order of these rotations matters.

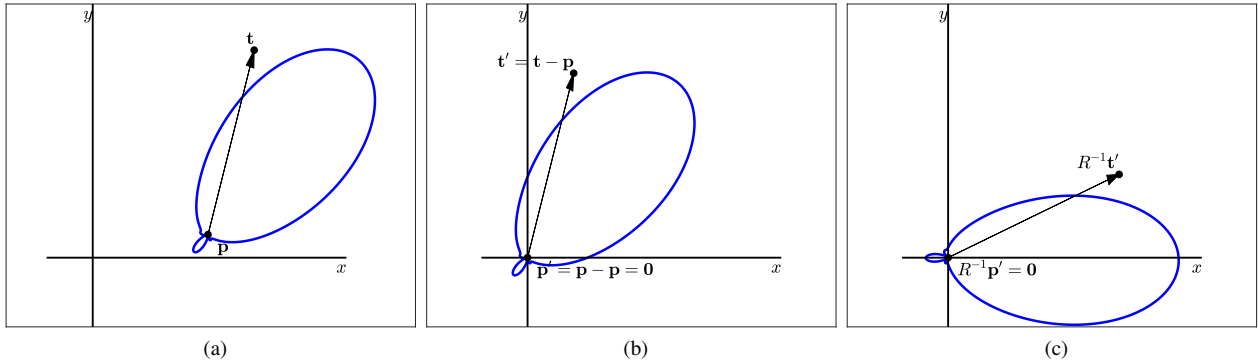


Fig. 4. An example illustrating the direction of departure. From (a) to (b), we translate the system by $-\mathbf{p}$ so that the position of the antenna is at the origin. From (b) to (c), we rotate by R^{-1} to align the main beam with the x -axis (the default orientation). This enables the evaluation of the gain function in a standardized way. In the opposite direction, we rotate the system by the orientation of the antenna R from (c) to (b) and then translate the system by the position of the antenna \mathbf{p} from (b) to (a).

(MDS) [44]. For convenience, we denote the MDS as τ^s and (linearly) express it as

$$\tau^s \triangleq \nu(\text{SNR}_{\text{out}})k_B B T. \quad (4)$$

Remark 1. The power of the emitter signal arriving at the sensor antenna must be larger than the threshold τ^s in order for the sensor to distinguish the emitter signal from noise.

2) *Antenna Gain Pattern:* The gain of an antenna describes the degree to which the antenna converts input power into radio waves or vice versa [45]. To evaluate the antenna gain value, we require the position of the antenna ($\mathbf{p} \in \mathbb{R}^d$), the location of the target ($\mathbf{t} \in \mathbb{R}^d$), the rotation of the antenna from a conventional orientation ($R \in \mathbb{R}^{d \times d}$), and the operating frequency (f) as inputs to the gain function: $g(\mathbf{p}, R, \mathbf{t}, f)$. A plot of the gain as a function of direction displays the antenna's radiation pattern. Antennas are said to possess directionality² if the antenna gain $g(\cdot)$ is a non-uniform function of the direction of departure or arrival. In other words, as one moves around the antenna, the antenna gain changes. As illustrated in Fig. 4, the normalized direction of departure is

$$R^{-1} \frac{\mathbf{t} - \mathbf{p}}{\|\mathbf{t} - \mathbf{p}\|}. \quad (5)$$

We also note that the antenna gain is a function of frequency. Generally, an antenna is designed to operate at a particular frequency, and operation outside of that band is degraded by poor gains or high reflection coefficients [45]. Consider as a simple example, a half-wave dipole antenna. If we double the operating frequency, the antenna becomes a full wave dipole antenna, which has a different pattern than a half-wave dipole.

For the two-dimensional case, the analysis of the inputs $(\mathbf{p}, R, \mathbf{t})$ reduces to the azimuth angle of departure, which we find as $\phi = \arctan\left(\frac{[0 \ 1]R^{-1}(\mathbf{t}-\mathbf{p})}{[1 \ 0]R^{-1}(\mathbf{t}-\mathbf{p})}\right)$, where care needs to be taken that the proper quadrant is selected for a unique solution (see `atan2` in many software packages). See Fig. 5 for an example of a two-dimensional directional antenna radiation

pattern. Note how the gain is large in one particular direction (at $\phi = 0$) and diminishes in other directions.

We simplify the gain patterns of the sensors and emitters in the following way. Let Ψ denote the half power beamwidth (HPBW) of a directional antenna. The HPBW is defined as the angular range between the points at which the gain has decreased 3 dB from the peak gain [45]. Also note that the HPBW is a function of the operating frequency, $\Psi(f)$, whose form is specific to the antenna. We simplify the gain to be constant within the HPBW and zero elsewhere. See Fig. 5 for an example of our simplification, which captures the essence of directional antennas. The simplified gain is always less than or equal to the true gain. Consequently, detection requires more restrictive circumstances under this simplification, which we address later in Sec. IV.

The HPBW and maximum gain of an antenna are physically related [45]. In general, as the HPBW narrows, the maximum gain increases. Consequently, the non-zero constant gain in our simplification is a function of the antenna beamwidth, both in azimuth and elevation. In this paper, we consider the scenario in which the sensors and emitters are approximately coplanar, which is well-modeled by our two-dimensional framework. Consequently, we treat elevation as constant and only vary the azimuth beamwidth Ψ . To be thorough, we include the elevation beamwidth Θ to show the relationship to gain, though Θ is effectively a constant. Without loss of generality, we assume antenna efficiencies of 1 so that antenna directivity equals gain. Our simplification is

$$g(\mathbf{p}, R, \mathbf{t}, f) = \begin{cases} \frac{1}{2} \frac{4\pi}{\Psi(f)\Theta(f)}, & \arctan\left(\frac{[0 \ 1]R^{-1}(\mathbf{t}-\mathbf{p})}{[1 \ 0]R^{-1}(\mathbf{t}-\mathbf{p})}\right) \in \left[-\frac{\Psi(f)}{2}, \frac{\Psi(f)}{2}\right] \\ 0, & \text{else,} \end{cases} \quad (6)$$

where \arctan is the four-quadrant inverse tangent. The expression $4\pi/\Psi(f)\Theta(f)$ is an approximation of the antenna's directivity that becomes more accurate with narrower beamwidths [45]. The factor of $1/2$ comes from using the 3 dB point as the constant value.

²The directionality of the antenna gain is usually accomplished through specialized antennas, such as a horned antenna, or through a phased array of multiple antennas.

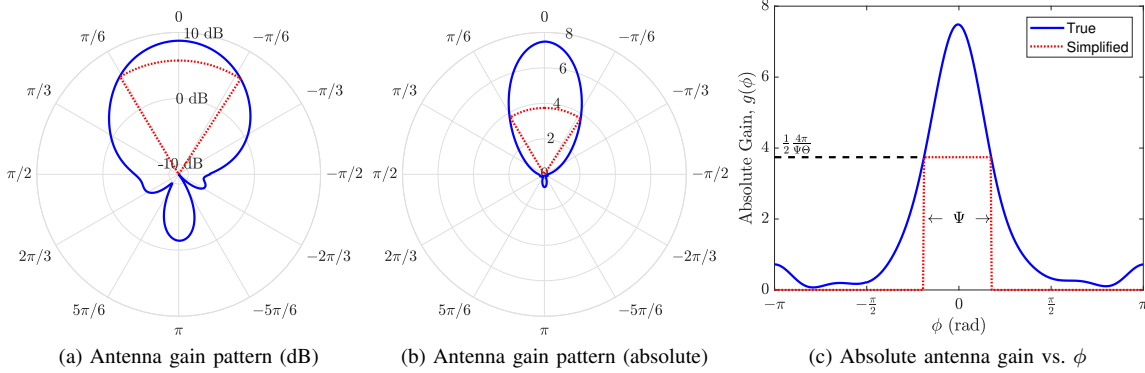


Fig. 5. An example antenna gain pattern (solid blue) from MATLAB's toolbox compared to our simplified radiation pattern (dotted red). The patterns are shown in dB in (a) and absolute values in (b). A Cartesian view of the absolute gain is in (c).

C. RF Channel

The channel is the medium over which the emitters transmit and the sensors receive radio waves. In wireless communications, the channel model incorporates aspects of the environment such as large-scale shadowing and small-scale fading, which determine how the radio wave changes from the emitter antenna to the sensor antenna. From the system perspective, we can incorporate the emitter and sensor gains into the channel.

For ease and wide applicability, we use the approximation given by the simplified path loss model in [24, Eq. 2.28]. Let us briefly define some notation. Let p_{ij}^s be the power received by sensor j from emitter i . Let $\|\mathbf{x}_i^e - \mathbf{x}_j^s\|$ denote the Euclidean distance between the i th emitter and j th sensor. Let $\alpha \geq 2$ be the path loss exponent determining the rate of power attenuation. Let h_{ij} be the fading coefficient for the channel between the i th emitter and j th sensor. h_{ij} could be the product of a small-scale fading and a shadowing random variable. This paper focuses on iid h_{ij} . We have

$$p_{ij}^s = h_{ij} g_j^s(\mathbf{x}_j^s, R_j^s, \mathbf{x}_i^e, f) g_i^e(\mathbf{x}_i^e, R_i^e, \mathbf{x}_j^s, f) \kappa(f) \|\mathbf{x}_i^e - \mathbf{x}_j^s\|^{-\alpha} p_i^e, \quad (7)$$

where $\kappa(f)$ incorporates other aspects of signal attenuation and antenna characteristics. A common form of $\kappa(f) = (c/4\pi f r_0)^2 r_0^\alpha$, where r_0 is a reference distance [24], [46]. If $h_{ij} \equiv 1$ and $\alpha = 2$, this choice of $\kappa(f)$ results in Friis equation for free space. Other choices of $\kappa(f)$ and α can result in the two-ray model, the Hata model, and the COST extension to the Hata model [24]. Without loss of generality, we set the frequency f constant throughout the derivations to simplify notation.

Finally, we note that the power at the input of the receiver of the j th sensor within a given bandwidth is given by

$$p_j^s \triangleq \sum_{i=1}^{n^e} p_{ij}^s + N_0, \quad (8)$$

where $N_0 = \nu k_B T B$ accounts for thermal noise and the receiver noise figure. For a single emitter, p_j^s is simply (7) with N_0 added. Without a priori knowledge of n^e , interpretations on p_j^s alone can be complicated if $n^e > 1$. Consequently, for the case of multiple emitters, we consider scenarios in which

the sensors have the capabilities to separate emitter signals and powers via low-level signal processing. As Sec. II-B mentioned, several previous works have implemented such signal processing and can provide estimates \widehat{p}_{ij}^s . To maintain generality, this paper does not specify a particular method by which sensors distinguish among multiple emitters, but we assume the capability in order to analyze the effects of multiple emitters on system design in Sec. IV. For simplicity of exposition, we consider scenarios in which the estimate can effectively be given by the already-approximated path loss model in (7).

We also note that the receiver chain of the sensor will introduce additional noise, which is accounted for by the noise figure ν of the sensor. As a result, we use the sensor MDS τ^s from (4) when evaluating whether the sensor can distinguish any emitter signal from noise. We consider scenarios in which sufficient time-averaging occurs such that the estimated noise floor is effectively the value of the true noise floor and τ^s can be treated as a constant threshold for detection. We note here that while finite-duration sampling inherently results in variation in the measured noise power, the variance becomes negligible with a reasonably high number of samples. Specifically, let the discrete-time samples of thermal noise, $w(n)$, be iid zero-mean Gaussian random variables with variance N_0 . The measured noise power is given by $Z = \frac{1}{K} \sum_{n=0}^{K-1} |w(n)|^2$, and Z has a gamma distribution with mean N_0 and variance $2N_0/K$. For large K , the variance becomes negligible, and the measured power is effectively given by N_0 .

D. Problem Statement

With the model, we can now mathematically define detection and state our problem.

Definition 1 (Detection by Sensor). *Detection occurs if a sensor distinguishes an emitter signal from noise. From the definition of τ^s in (4), the j th sensor detects the i th emitter if and only if*

$$p_{ij}^s \geq \tau^s. \quad (9)$$

Here we note that the sensors employ a fixed threshold for detection, which arises from the limiting scenario in which sufficient time-averaging occurs such that the sensor

measurement of the noise floor is effectively the true noise floor, N_0 . In terms of the probability of detection and false alarm, we want to find P_D for the sensors operating at $P_F = 0$. The threshold τ^s can be adjusted (via arbitrary SNR_{out}) to be greater than N_0 such that $P_F \rightarrow 0$ for an individual sensor as K grows. Nonetheless, if $P_F > 0$, the fusion of sensor data via an OR function at the network level would cause the network false alarm rate to approach 1 as the number of sensors grows. Consequently, a more sophisticated fusion method of sensor data (e.g., fusion of soft decisions, sensor reputation, measurement confidence, and/or verification by nearby sensors) would be required for very large deployments. This problem is outside the scope of this paper but has been considered thoroughly in other works (e.g., [47], [48] and sources therein). Additionally, different algorithms could be used for detection at the sensor level (e.g., variable thresholds) to lower P_F for a given P_D . With such algorithms, increasing the sensor density could also lower P_F for a given P_D . Thus, the results of this paper can be viewed as lower bounds on sensor density. Detailed analyses to incorporate such algorithms and the trade-offs between P_D and P_F are beyond the scope of this paper.

For a random deployment of sensors, we want to know the required sensor density to successfully detect unknown directional emitters. To this end, we begin with the relationship between the deployment density of sensors λ^s and the probability that at least one sensor detects a single emitter. Let us mathematically define detection by a sensor network.

Definition 2 (Detection by Sensor Network). *The sensor network detects an emitter if at least one sensor detects the emitter. We express the event that the sensor network detects the i th emitter as*

$$\mathcal{E}_i \triangleq \bigcup_j \{p_{ij}^s \geq \tau^s\}. \quad (10)$$

Remark 2. For the case of a single emitter, we assume the emitter to be at the origin o . Since the sensor locations form a stationary PPP, there is no loss of generality. The notation for sensor network detection simplifies to \mathcal{E} . If emitters form an arbitrary stationary point process independent of Φ^s , the emitter at o is the typical emitter.

Starting with the case of a single emitter, we want to find the relationship $\Pr(\mathcal{E}) = f(\lambda^s)$ for a function f . If f is invertible, we can find $\lambda^s = f^{-1}(\Pr(\mathcal{E}))$ for a given confidence. For multiple emitters, we can apply the same strategy with the event $\mathcal{D} \triangleq \bigcap_i \mathcal{E}_i$ by finding the relationship between λ^s and $\Pr(\mathcal{D})$.

III. RESULTS FOR SINGLE EMITTER

A. General Result

Proposition 1. Let Φ be a stationary PPP of intensity λ and $(M_{\mathbf{x}})_{\mathbf{x} \in \Phi}$ a family of iid non-negative random variables (marks), independent of Φ , with finite moment $\mathbb{E}[M_{\mathbf{x}}^{2/\alpha}]$. For $\theta > 0$, the random variable

$$N \triangleq \sum_{\mathbf{x} \in \Phi} \mathbb{1}[M_{\mathbf{x}} \|\mathbf{x}\|^{-\alpha} > \theta] \quad (11)$$

is Poisson with mean

$$\mathbb{E}[N] = \lambda \pi \theta^{-\delta} \mathbb{E}[M^\delta], \quad (12)$$

where M is distributed like all $M_{\mathbf{x}}$ and $\delta = 2/\alpha$. In particular,

$$\begin{aligned} \Pr(N > 0) &= 1 - \exp(-\mathbb{E}[N]) \\ &= 1 - \exp(-\lambda \pi \theta^{-\delta} \mathbb{E}[M^\delta]). \end{aligned} \quad (13)$$

Proof: Let \bar{F}_M denote the complementary cumulative distribution function of M . N is the cardinality of the point process $\Phi' = \{\mathbf{x} \in \Phi: M_{\mathbf{x}} > \theta \|\mathbf{x}\|^\alpha\}$. Since the $M_{\mathbf{x}}$ are iid, Φ' is an independently thinned version of Φ and thus itself a PPP [32, Thm. 2.36]. The thinning probability of a point at \mathbf{x} is $\mathbb{E}_M[\mathbb{1}[M_{\mathbf{x}} > \theta \|\mathbf{x}\|^\alpha]] = \bar{F}_M(\theta \|\mathbf{x}\|^\alpha)$. Hence, Φ' has the density function $\lambda'(\mathbf{x}) = \lambda \bar{F}_M(\theta \|\mathbf{x}\|^\alpha)$. The mean number of points in Φ' follows as

$$\begin{aligned} \mathbb{E}[N] &= \int_{\mathbf{x} \in \mathbb{R}^2} \lambda'(\mathbf{x}) \, d\mathbf{x} \\ &= \lambda \int_{\mathbf{x} \in \mathbb{R}^2} \bar{F}_M(\theta \|\mathbf{x}\|^\alpha) \, d\mathbf{x} \\ &= 2\pi\lambda \int_0^\infty \bar{F}_M(\theta r^\alpha) r \, dr \\ &= \lambda \pi \theta^{-\delta} \int_0^\infty \delta u^{\delta-1} \bar{F}_M(u) \, du \\ &= \lambda \pi \theta^{-\delta} \mathbb{E}[M^\delta]. \end{aligned} \quad (14)$$

The fourth line is obtained by the substitution $u = \theta r^\alpha$. Since $\mathbb{E}[M^\delta]$ is finite, $\mathbb{E}[N]$ is finite, and thus N is Poisson distributed. \square

Remark 3. If $\mathbb{E}[M] \neq 1$, we can set $M'_{\mathbf{x}} = M_{\mathbf{x}}/\mathbb{E}[M]$ and adjust θ to $\theta/\mathbb{E}[M]$, thereby normalizing $\mathbb{E}[M]$ to 1 without loss of generality. If $\mathbb{E}[M] = 1$, then $\mathbb{E}[M^\delta] < 1$. Therefore, randomness (e.g., fading, shadowing, and/or directional orientation) never helps detection.

We present the following applications of the proposition to our problem statement. Let N denote the number of sensors whose received power matches or exceeds τ^s . Therefore, $\mathcal{E} = \{N > 0\}$. $M_{\mathbf{x}}$ is a random variable which incorporates fading and the directionality of the randomly oriented emitter and sensor. Finally, let θ be an arbitrary received-power threshold whose form depends on the scenario. We assume the emitter at the origin o transmits at power p^e . Without loss of generality, we assume $\kappa = 1$ below (p^e can be replaced by κp^e).

B. Applications

1) *Baseline: Isotropic Emitter and Sensors, No Fading:* For isotropic transmission and reception without fading, $\theta = \tau^s/p^e$, $M_{\mathbf{x}} \equiv 1$, and the gains are unity. Thus,

$$\Pr(\mathcal{E}) = 1 - \exp(-\lambda^s \pi (p^e/\tau^s)^\delta). \quad (15)$$

2) *Directional Emitter, No Fading:* Here the emitter transmits directionally, in an angle fraction $\eta^e = \Psi^e/(2\pi)$, which results in an independent thinning of the PPP by η^e and a power gain $(\eta^e \Theta^e)^{-1}$. Hence,

$$\Pr(\mathcal{E}) = 1 - \exp(-\lambda^s \eta^e \pi (p^e/(\eta^e \Theta^e \tau^s))^\delta). \quad (16)$$

3) *Directional Sensors, No Fading*: In this case, the marks model the random orientation of the sensors. Due to the 0-1 nature of the gain function, either a sensor is oriented toward the emitter and receives the signal, or a sensor is directed away from the emitter and cannot detect the emitter. This behavior is captured with a Bernoulli random variable whose mean is the fraction of emitter-detecting orientations. Consequently, the marks are Bernoulli with mean $\eta^s = \Psi^s/(2\pi)$. Hence, $\mathbb{E}[M^\delta] = \eta^s$. The power gain is $(\eta^s \Theta^s)^{-1}$, and we obtain

$$\Pr(\mathcal{E}) = 1 - \exp(-\lambda^s \eta^s \pi (p^e / (\eta^s \Theta^s \tau^s))^\delta). \quad (17)$$

Hence, directionality at the transmitter and directionality at the receiver have the same effect on the detection probability.

4) *Directional Emitter and Sensors, No Fading*: Combining the two previous results, we obtain

$$\Pr(\mathcal{E}) = 1 - \exp(-\lambda^s \eta^e \eta^s \pi (p^e / (\eta^e \eta^s \Theta^e \Theta^s \tau^s))^\delta). \quad (18)$$

5) *Omnidirectional Emitter with Fading*: With iid fading, the marks represent the fading coefficients, and we observe from (13) that the effect of fading is equivalent to an adjustment in the density of the PPP, by a factor corresponding to the δ -th moment of the fading random variables.

For Rayleigh fading, where the $M_{\mathbf{x}}$ are exponential with mean 1, we have $\mathbb{E}[M^\delta] = \Gamma(1+\delta)$, where the gamma function $\Gamma(z) \triangleq \int_0^\infty t^{z-1} e^{-t} dt$. Substituting $\mathbb{E}[M^\delta] = \Gamma(1+\delta)$ into (13) provides

$$\Pr(\mathcal{E}) = 1 - \exp(-\lambda^s \pi \Gamma(1+\delta) (p^e / (\Theta^e \tau^s))^\delta). \quad (19)$$

Since $\Gamma(1+\delta) < 1$ for $\alpha > 2$, Rayleigh fading has a negative effect on the detection probability.

Alternatively, the effect of fading can be viewed as a scaling of the transmit power by $(\mathbb{E}[M^\delta])^{1/\delta}$. Interestingly, in the case of Rayleigh fading, this power “gain” $\Gamma(1+\delta)^{1/\delta}$ is tightly lower bounded by $1/2 + \delta/2$. If the power is increased by $2/(1+\delta) = 2\alpha/(\alpha+2)$, the effect of Rayleigh fading is compensated (slightly overcompensated, actually).

If (small-scale) fading and shadowing are both present, then $M_{\mathbf{x}}$ can be taken to be the product of both random variables.

6) *Directional Emitter and Sensors with Fading*: Here the marks represent the combined effect of directional reception and fading. Denoting the Bernoulli random variables for directionality by $b_{\mathbf{x}}$ and the fading coefficients by $h_{\mathbf{x}}$, we have $M_{\mathbf{x}} = b_{\mathbf{x}} h_{\mathbf{x}}$ and $\mathbb{E}[M^\delta] = \eta^s \mathbb{E}[h^\delta]$. As before, directional transmission is taken into account by thinning the PPP by η^e . We obtain

$$\Pr(\mathcal{E}) = 1 - \exp(-\lambda^s \eta^e \eta^s \pi \mathbb{E}[h^\delta] (p^e / (\eta^e \eta^s \Theta^e \Theta^s \tau^s))^\delta). \quad (20)$$

This is the most general form for $\Pr(\mathcal{E})$ from which the previous equations can be derived by proper substitution. Also note that all results depend on the ratio of the channel parameters $C \triangleq \kappa p^e / (\Theta^e \Theta^s)$. Further, only the ratio $\omega \triangleq C / \tau^s$ matters. Therefore, (20) could be concisely written as $\Pr(\mathcal{E}) = 1 - \exp(-\lambda^s \eta^e \eta^s \pi \mathbb{E}[h^\delta] (\omega / (\eta^e \eta^s))^\delta)$.

7) *Other Point Processes*: Here we consider point processes that are more or less regular than the PPP. The PPP exhibits *complete spatial randomness* [32, Sec 3.1]. In contrast, point processes such as soft-core and hard-core processes exhibit repulsion between points, with the limit being a lattice. In the other direction, cluster point processes exhibit attraction between points. The PPP is the mid-point on this general spatial regularity scale with no interaction among its points.

If the sensor locations form a cluster point process, we can use the result for the PPP as an upper bound on the detection probability. Intuitively, clustering increases the amount of overlap among the sensor coverage regions. For a given density of sensors, as clustering increases, the performance degrades. On the other hand, as we decrease the amount of clustering, say for a Neyman-Scott process whose clusters are translated to points of a PPP [32, Def. 3.4], the point process will approach a PPP.

For crowdsourced sensors, only a subset can be expected to participate in sensing. Even if the sensor locations are clustered, an independent thinning of the process will be close to a PPP in some scenarios [49, Sec. 3.3]. Therefore, it is still reasonable to use the PPP model for crowdsourcing.

If there is a possibility of designing the distribution of the sensor locations, more regular point processes perform better than the PPP. Let us again consider the baseline case of an isotropic emitter and isotropic sensors with no fading. The distribution that would achieve the highest detection probability for a given λ^s is the triangular lattice point process [50]. In particular, let the sensors have sensing radius $\rho = (p^e / \tau^s)^{1/\alpha}$. If the lattice spacing is a , then $\lambda^s = 2/(a^2 \sqrt{3})$. If $a \geq 2\rho$, then the detection probability is at most $\lambda^s \pi (p^e / \tau^s)^\delta$, and if $a \leq \rho \sqrt{3}$, then the detection probability can reach 1 [50].

The triangular lattice does indeed perform better than a PPP of sensor locations. For a PPP, $\Pr(\mathcal{E}) = 1 - \exp(-\lambda^s \pi (p^e / \tau^s)^\delta)$. Both 1 and $\lambda^s \pi (p^e / \tau^s)^\delta$ for a triangular lattice match or exceed the PPP's value because $x \geq 1 - e^{-x}$ for $x \geq 0$.

While the triangular lattice could be a target distribution, in practice variance from the lattice would exist. In particular, a reasonable point process model could be a perturbed lattice with each location having a two-dimensional Gaussian shift from the triangular lattice [32, Def. 2.16]. However, a closed-form expression for $\Pr(\mathcal{E})$ for a perturbed lattice is elusive. Nonetheless, since the triangular lattice achieves the best possible $\Pr(\mathcal{E})$ for a given λ^s [50], its performance can be treated as a bound for such deployment distributions. Further, the perturbed lattice quickly approaches a PPP if it is likely that a point is displaced by more than twice the mean nearest-neighbor distance [51, Sec. II.C].

8) *Unknown Emitter Gain*: The assumption that the emitter's gain function is known may not always hold. With Prop. 1, only the statistics of the emitter pattern need to be known. In this case, we treat g^e as random with distribution f_g . Here the marks represent the combined effect of the fading ($h_{\mathbf{x}}$), directional reception ($b_{\mathbf{x}}$), and unknown emitter gain (g^e). In particular, $M_{\mathbf{x}} = b_{\mathbf{x}} h_{\mathbf{x}} g^e$, and $\mathbb{E}[M^\delta] = \mathbb{E}[(b h g^e)^\delta]$. If f_g is independent of fading and sensor orientations, $\mathbb{E}[M^\delta] =$

$\eta^s \mathbb{E}[h^\delta] \mathbb{E}[(g^e)^\delta]$. The result is

$$\Pr(\mathcal{E}) = 1 - \exp(-\lambda^s \eta^s \pi \mathbb{E}[h^\delta] \mathbb{E}[(g^e)^\delta] (p^e / (\eta^s \Theta^s \tau^s))^\delta). \quad (21)$$

From Remark 3, this additional randomness decreases the detection probability. For multiple emitters, an additional assumption that the g_i^e are iid would be needed for the results to hold in Sec. IV.

C. Observations

Let us observe the behavior of (20). Note that if the path loss exponent $\alpha = 2$, which corresponds to free space, the azimuth beamwidths Ψ^s and Ψ^e do not affect $\Pr(\mathcal{E})$. This rather surprising result states that if the environment is free space, the choice of (azimuth) directivity does not matter. Intuitively, when beamwidth decreases, the antenna gain and thereby the transmission range increase. However, if $\alpha = 2$, the extension of the range is such that the area of the average coverage sector remains constant.

Let us also observe the influence of the parameters on $\Pr(\mathcal{E})$. The probability is most sensitive to the sensor density λ^s . The only exception is in the case of free space ($\alpha = 2$) for which the sensor density is equally influential as the ratio of system parameters ω . As the path loss exponent α increases, $\Pr(\mathcal{E})$ becomes more sensitive to azimuth beamwidth Ψ . On the other hand, as α decreases, $\Pr(\mathcal{E})$ becomes more sensitive to the variable ω .

Ultimately, we want to know the density of sensors to deploy in order to be confident that we detect the emitter present. Equation (20) provides us with a metric for system design trade-offs. If we set a desired $\Pr(\mathcal{E}) = \beta$, we rearrange (20) to obtain

$$\lambda^s = \frac{\ln\left(\frac{1}{1-\beta}\right)}{\eta^e \eta^s \pi \mathbb{E}[h^\delta] (\omega / (\eta^e \eta^s))^\delta}. \quad (22)$$

We see from (22) that the required sensor density $\lambda^s \propto \left(\frac{1}{\Psi^e}\right)^{1-\delta}$. In other words, as the emitter becomes more directional (*i.e.*, as $\Psi^e \rightarrow 0$), the sensor density needs to increase, specifically by a factor of $\left(\frac{1}{\Psi^e}\right)^{1-\delta}$. Hence, the directivity of the emitter(s) has a significant influence on the design and deployment of the spectrum monitoring system. In particular, we see that with $\alpha = 4$ and all other things equal, quartering the emitter HPBW doubles the average number of sensors needed for detection: $\lambda^s \propto \left(\frac{1}{\Psi^e/4}\right)^{1/2} = 2 \left(\frac{1}{\Psi^e}\right)^{1/2}$.

In practice, the deployment of sensors is limited by cost, and deploying more sensors increases the total cost. For a set probability, we can decrease the sensor density in (22) by maximizing the sensor beamwidth Ψ^s to 2π . We can also decrease λ^s by decreasing the sensor elevation beamwidth Θ^s , but we are slightly constrained. Ideally, we would let $\Theta^s \rightarrow 0$, but such antennas do not physically exist, and if $\Theta^s \rightarrow 0$, the sensors would need to be exactly coplanar, which is impractical. Ultimately, this analysis suggests that the sensors should be designed with omnidirectional antennas with $\Psi^s = 2\pi$.

Next, we consider the sensor MDS τ^s . For a given $\Pr(\mathcal{E})$, lowering τ^s can allow a decrease in λ^s . However, lowering

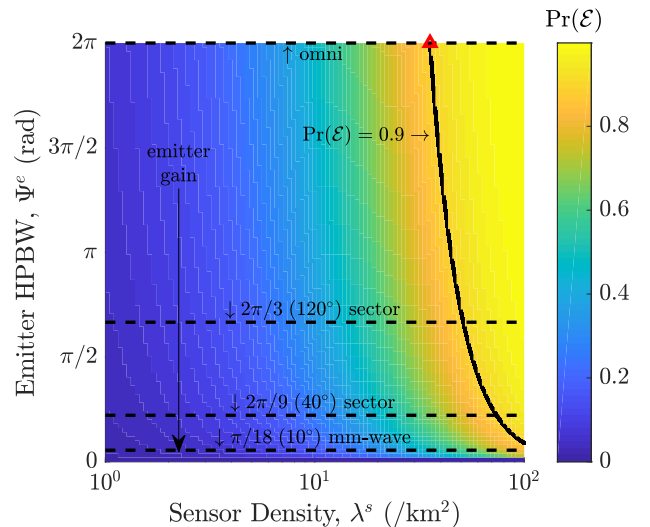


Fig. 6. The probability of emitter detection by the sensor network as a function of sensor density (λ^s) and emitter HPBW (Ψ^e), given by (20). We use the parameters in Table II.

τ^s generally increases the cost of each sensor. Usually the RF environment is not free-space ($\alpha = 2$), so $\Pr(\mathcal{E})$ is less sensitive to the sensor MDS τ^s than the sensor density λ^s . Therefore, for a fixed budget, we improve $\Pr(\mathcal{E})$ by letting τ^s be higher for a lower cost sensor and then increasing λ^s . In other words, we lower the cost of the sensor in order to deploy more of them. The larger density of sensors improves $\Pr(\mathcal{E})$ more than the degradation from a higher MDS. We present an example in a later section.

We plot (20) in Fig. 6 for Rayleigh fading and the example parameters listed in Table II. For the sensor sensitivity, we experimentally measured a RadioHound sensor to find a minimum detectable signal of around -110 dBm [20]. For representative emitters, we consider a dipole (omnidirectional), a traditional cell tower sector antenna ($\Psi^e = 2\pi/3$ rad), a narrower sector antenna ($\Psi^e = 2\pi/9$ rad), and a mm-wave antenna ($\Psi^e = \pi/18$ rad). Fig. 6 shows that a higher sensor density is needed to maintain a constant $\Pr(\mathcal{E})$ for increasing emitter directivity. The red triangle indicates the approach to calculate the sensor deployment density to achieve $\Pr(\mathcal{E}) = 0.9$ under the assumption that the emitter is omnidirectional. For the same $\Pr(\mathcal{E})$, this paper also accounts for the emitter HPBW and calculates the sensor density indicated by the solid black line. For instance, if the system is designed for an omnidirectional emitter but the emitter uses a mm-wave antenna, the sensor density would need to more than triple, or $\Pr(\mathcal{E})$ would decrease to about 0.5.

D. Frequency Sensitivity and Multiple Frequency Bands

We return to the fact that Ψ , Θ , and κ in the previous expressions are frequency-dependent. In practice, we have to design the sensor network to operate at a given frequency and design the antennas to have appropriate beamwidths. Once the sensors are deployed and the geometry of their antennas is fixed, the performance of the network is sensitive to emitter frequency. For the case of no fading, our study of

TABLE II
PARAMETERS FOR SIMULATIONS

Parameter	Value
Sensor azimuth beamwidth, Ψ^s	2π rad
Sensor elevation beamwidth, Θ^s	$\pi/2$ rad
Sensor MDS, τ^s	-110 dBm
Emitter elevation beamwidth, Θ^e	$\pi/2$ rad
Emitter transmission power, p^e	0 dBm
Frequency, f	1 GHz
Path loss exponent, α	3
Fading, h	Rayleigh, $h \sim \exp(1)$

the sensitivity indicates that the values of (20) and (22) are not significantly affected if the change in frequency relative to the original operating frequency ($\Delta f/f$) is small. In particular, let $\bar{\mathcal{E}}$ denote the complement of \mathcal{E} . If we perturb the designed operating frequency from f to $f + \Delta f$, and $|\Delta f/f| \ll 1/2$, then

$$\Pr(\bar{\mathcal{E}})|_{f+\Delta f} \approx (\Pr(\bar{\mathcal{E}})|_f)^\xi, \quad (23)$$

where $\xi = 1 - 2(1 - \delta)\Delta f/f$ [52, Ch. 4]. From our previous example for omnidirectional sensors and emitters with $\lambda^s = 50/\text{km}^2$, the relative change of $\Pr(\mathcal{E})$ is less than 1% if $-0.13 < \Delta f/f < 0.10$. In other words, at a carrier frequency of 1 GHz, the frequency can range from 870 MHz to 1100 MHz with less than a 1% change in $\Pr(\mathcal{E})$. Further details and analysis are available in [52].

For a relative change in frequency $\Delta f/f$, we could maintain approximately the same performance with a relative change in sensor density $\Delta\lambda^s/\lambda^s$:

$$\Delta\lambda^s/\lambda^s = (1 - \xi)/\xi. \quad (24)$$

If $\Delta f/f < 0$, then $\Delta\lambda^s/\lambda^s < 0$. Intuitively, the coverage of the sensors increases with decreasing operating frequency, thereby requiring fewer sensors. Therefore, to design a deployment for the frequency range f_1 to f_2 , we should deploy the λ^s required for f_2 . The performance for the remainder of the band will be equivalent to or better than that of f_2 , or a subset of sensors could be used for the lower bands such that the desired detection probability is achieved.

E. Fixed-Budget Example

We return to the observation made in a previous section that the sensor MDS τ^s does not influence the probability of detection $\Pr(\mathcal{E})$ as strongly as sensor density λ^s if $\alpha > 2$. For a fixed monetary budget, one could lower the sensor cost by increasing the sensor MDS and thereby deploy more sensors to increase the probability of detection.

Our motivation is a low SWaP-C (size, weight, power, and cost) RF sensor that costs on the order of a dollar [20]. The ideal is to have the sensor incorporated into widely deployed technologies, such as cell phones, tablets, WiFi access points, smart appliances, etc. Such devices have a dedicated power supply or are regularly recharged by users. The incentive to pay the slight overhead to include the sensor in devices is spectrum as a service [53]. In other words, the collected data will enable better spectrum management and usage, thereby improving user experience. In militarized contexts, the sensors

TABLE III
SOFTWARE DEFINED RADIOS

Radio	Cost	Noise Figure	Label
RadioHound	\$ 20	10 dB	A
Ettus USRP B205mini	\$ 910	8 dB	B
NI USRP 2900	\$ 1,031	7 dB	C
Ettus USRP N310	\$ 10,000	6.8 dB	D
NI USRP 2945	\$ 11,503	5 dB	E
Airspy Mini	\$ 100	3.5 dB	F
Airspy R2	\$ 250	3.5 dB	G
AD9364 RFIC	\$ 400	2.5 dB	H

are inexpensive enough to be disposable. The military would not try to retrieve or maintain them. Hence, we can disregard the cost of maintenance and battery replacement here.

We consider the cost and MDS of several current representative software defined radios (SDRs) in Table III from Ettus Research, National Instruments, and Airspy, along with the RadioHound sensor from [20]. Several SDRs share the same MDS, so we select the lowest priced one and omit the rest. The reason is that the higher-priced SDRs for a given MDS have other benefits not considered by our model, such as a larger dynamic range. We determine the MDS of each SDR via (4) with an SNR_{out} of 1 and standard temperature of 290 K. For each SDR, we assume the worst-case noise figure for a frequency of 1 GHz given in its specifications. We use a bandwidth of 2.56 MHz for all systems, limited by the sampling rate of the RadioHound sensor [20].

We plot (4) in Fig. 7a for the SDRs in Table III. We observe two clusters of SDRs, each with the trend of decreasing MDS with increasing cost. The clusters result due to other factors in the SDRs that affect price, such as sampling rate, filtering capabilities, dynamic range, etc.

Next, we consider a deployment with a limited budget of \$1000 per km^2 . Based on this budget and the price of the SDR sensor, we can calculate the sensor density λ^s . Using the parameters in Table II for omnidirectional sensors and emitters, we plot $\Pr(\mathcal{E})$ in (20) as a function of the sensor cost in Fig. 7b. We have normalized the SDR cost by other factors, including the number of receiver chains, number of RF ports, resolution of the ADC, sampling bandwidth, and frequency range. For all cases, we observe the same trend but with different slopes (m). Decreasing sensor cost increases $\Pr(\mathcal{E})$. In comparison with Fig. 7a, we see that sensors of similar cost have a very similar $\Pr(\mathcal{E})$ despite the significant difference in MDS. In other words, we see that for a fixed budget, the sensor cost is a large factor in the metric $\Pr(\mathcal{E})$, whereas the MDS is not as influential. In particular, we fit an approximately linear relationship in Fig. 7b for which decreasing the individual sensor cost by a factor of 10 roughly increases the probability of detection by about a factor of 10. We then observe diminishing returns on $\Pr(\mathcal{E})$ as the sensor cost becomes very low.

Overall, this example supports decreasing sensor quality to decrease cost and thereby increase the sensor quantity. Other experiments are consistent with this theoretical result [6], [17], [53].

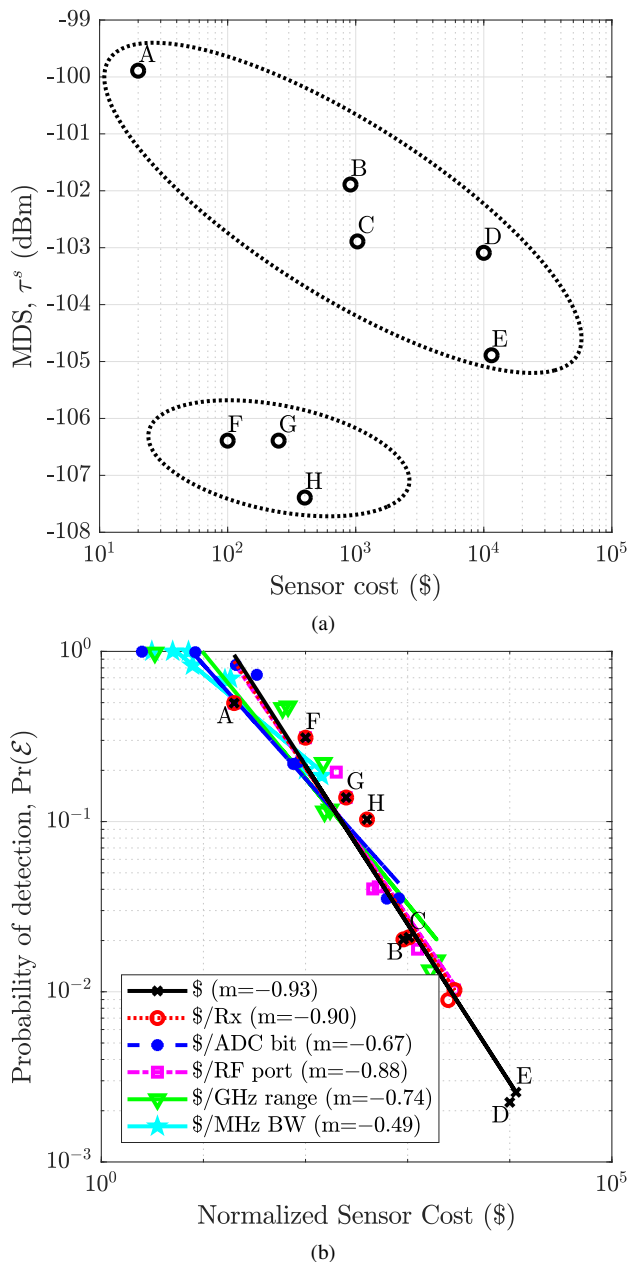


Fig. 7. An example illustrating the trade-off between the sensor MDS and $\Pr(\mathcal{E})$ for a fixed budget of \$1000 per km^2 . The plot in (a) shows the MDS from (4) versus sensor cost for the representative RF sensors in Table III. For these sensors, (b) shows $\Pr(\mathcal{E})$ from (20) as a function of sensor cost normalized by various hardware characteristics. The fitted curves have slopes given by m . The Table II parameters and omnidirectional antennas are used.

IV. RESULTS FOR MULTIPLE EMITTERS

A. Lower Bound on $\Pr(\mathcal{D})$

For n^e emitters arbitrarily located in a finite region \mathcal{R} , we want the probability that each emitter is detected by at least one sensor. Mathematically, we are interested in the event

$$\mathcal{D} \triangleq \bigcap_{i=1}^{n^e} \mathcal{E}_i. \quad (25)$$

However, the events \mathcal{E}_i are dependent. As a simple example, consider two omnidirectional emitters. If the second emitter is near the first, \mathcal{E}_1 occurring would affect the detection

probability for the second emitter. Unfortunately, the general dependence is complicated and has eluded analysis.

Instead, we derive a lower bound on $\Pr(\mathcal{D} | n^e)$ with DeMorgan's Law and the union bound:

$$\begin{aligned} 1 - \Pr(\mathcal{D} | n^e) &= \Pr(\mathcal{D}^c | n^e) = \Pr\left(\bigcup_{i=1}^{n^e} \mathcal{E}_i^c | n^e\right) \\ &\leq \sum_{i=1}^{n^e} \Pr(\mathcal{E}_i^c). \end{aligned} \quad (26)$$

We rearrange the terms and find $\Pr(\mathcal{E}_i^c)$ from (20) for a single emitter:

$$\begin{aligned} \Pr(\mathcal{D} | n^e) &\geq 1 - \sum_{i=1}^{n^e} \Pr(\mathcal{E}_i^c) \\ &= 1 - n^e \exp(-\lambda^s \eta^e \eta^s \pi \mathbb{E}[h^\delta] (\omega / (\eta^e \eta^s))^\delta). \end{aligned} \quad (27)$$

If the emitter locations are modeled as an arbitrary stationary point process with density λ^e , $\Pr(\mathcal{D})$ is found by taking the expectation with respect to n^e with $\mathbb{E}[n^e] = \lambda^e |\mathcal{R}|$.

As an example, we use the parameters in Table II. Here we set the sensor density to $\lambda^s = 100$ sensors/ km^2 and vary the number of emitters n^e . We plot the bound of $\Pr(\mathcal{D} | n^e)$ in (27) as a function of the number of emitters in Fig. 8. We also plot the exact $\Pr(\mathcal{D} | n^e)$ via simulation. We highlight the following observations. Given that the emitters have the same parameters, we see from (27) that the lower bound on $\Pr(\mathcal{D} | n^e)$ is linear in n^e with slope $\exp(-\lambda^s \eta^e \eta^s \pi \mathbb{E}[h^\delta] (\omega / (\eta^e \eta^s))^\delta)$. The plot again demonstrates the benefit of omnidirectional sensors. In particular, we see that the lower bound for omnidirectional emitters and sensors is close to the upper bound of 1. Consequently, the true $\Pr(\mathcal{D} | n^e)$ is close to 1 for omnidirectional sensors and emitters in this example. We also note for desirable, high values of $\Pr(\mathcal{D} | n^e)$, the lower bound is fairly tight.

From (27), we can find an upper bound on the sensor density required for a given confidence of detection. In other words, if we select a desired $\Pr(\mathcal{D} | n^e) = a$, we find

$$\lambda^s \leq \frac{\ln\left(\frac{n^e}{1-a}\right)}{\eta^e \eta^s \pi \mathbb{E}[h^\delta] (\omega / (\eta^e \eta^s))^\delta}. \quad (28)$$

We observe (28) is logarithmic in n^e , suggesting that a slight increase in the sensor density is needed to detect more emitters. In other words, a significant effort is needed to detect one emitter, but the extra cost to detect several is marginal.

We also note that the lower bound in (27) is consistent with the approximations of our model. The simplified gain model in (6) results in power gains and angle-of-views smaller than the true ones. Mathematically, let $\widetilde{\Pr}(\mathcal{E})$ denote the exact probability, and let $\Pr(\mathcal{E})$ denote our model approximation of $\widetilde{\Pr}(\mathcal{E})$. We know $\widetilde{\Pr}(\mathcal{E}) \geq \Pr(\mathcal{E})$. Therefore, $\widetilde{\Pr}(\mathcal{E}^c) = 1 - \widetilde{\Pr}(\mathcal{E}) \leq 1 - \Pr(\mathcal{E}) = \Pr(\mathcal{E}^c)$. Consequently, in (27), we have $\Pr(\mathcal{D} | n^e) \geq 1 - \sum_{i=1}^{n^e} \widetilde{\Pr}(\mathcal{E}_i^c) \geq 1 - \sum_{i=1}^{n^e} \Pr(\mathcal{E}_i^c)$, which is consistent.

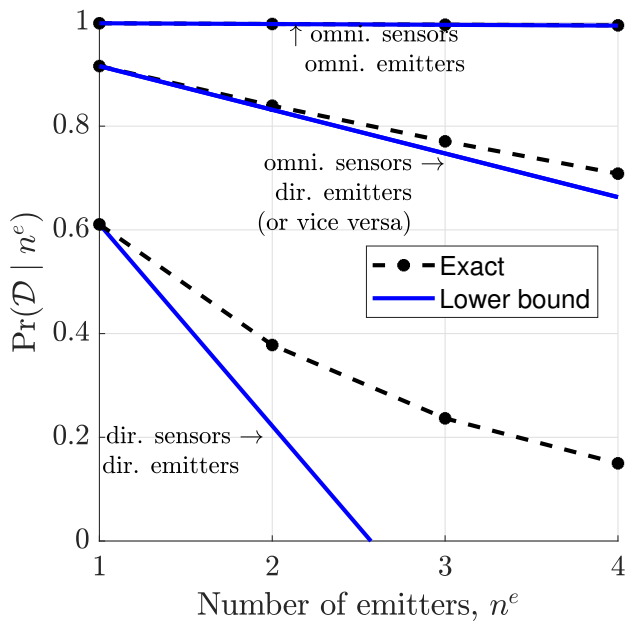


Fig. 8. The lower bound on the probability that the sensor network detects each of n^e emitters, given by (27). We use the parameters in Table II with a sensor density $\lambda^s = 100$ sensors/km². A directional sensor (or emitter) has an azimuth beamwidth of $\pi/9$ radians. An omnidirectional sensor (or emitter) has a beamwidth of 2π radians. The elevation beamwidth is set to $\pi/2$ radians for all cases. The exact $\Pr(\mathcal{D} | n^e)$ is found via simulation.

B. Expected Number of Undetected Emitters

If $\Pr(\mathcal{D})$ is low, the metric $\Pr(\mathcal{D})$ does not itself reveal how many emitters are not detected. Perhaps it is tolerable for the sensor network to detect all but one emitter. It can be difficult to interpret the situation solely with $\Pr(\mathcal{D})$. Here we propose another metric that may lend more insight. For n^e emitters arbitrarily located in a finite region \mathcal{R} , we consider the number of undetected emitters, $0 \leq n^u \leq n^e$. We can express $\mathbb{E}[n^u]$ analytically and use the result to design the system to drive $\mathbb{E}[n^u] \rightarrow 0$.

We express $n^u = \sum_{i=1}^{n^e} \mathbb{1}[\mathcal{E}_i^c]$, where $\mathbb{1}[\cdot]$ is the indicator function. Conditioned on the number of emitters in the region, we find $\mathbb{E}[n^u | n^e] = \mathbb{E}[\sum_{i=1}^{n^e} \mathbb{1}[\mathcal{E}_i^c] | n^e] = \sum_{i=1}^{n^e} \Pr(\mathcal{E}_i^c) = n^e \Pr(\mathcal{E}^c)$. Therefore,

$$\mathbb{E}[n^u | n^e] = n^e \exp(-\lambda^s \eta^e \eta^s \pi \mathbb{E}[h^\delta] (\omega / (\eta^e \eta^s))^\delta). \quad (29)$$

If the emitter locations are modeled as an arbitrary stationary point process with density λ^e , then $\mathbb{E}[n^u]$ is found by taking the expectation with respect to n^e with $\mathbb{E}[n^e] = \lambda^e |\mathcal{R}|$.

This expression is consistent with the following intuitive cases. As $\lambda^s \rightarrow \infty$ and/or $\omega \rightarrow \infty$, we have $\mathbb{E}[n^u] \rightarrow 0$. Additionally, as $\lambda^s \rightarrow 0$, $\eta^e \rightarrow 0$, $\eta^s \rightarrow 0$, and/or $\omega \rightarrow 0$, we have $\mathbb{E}[n^u] \rightarrow \mathbb{E}[n^e]$. The result reinforces our previous conclusions. To minimize $\mathbb{E}[n^u]$, we desire omnidirectional sensors ($\Psi^s = 2\pi$) with low MDS τ^s and high density λ^s .

As an application, $\mathbb{E}[n^u]$ could inform the required sensor density for scenarios in which it is tolerable to miss some number of emitters. Without loss of generality, we consider

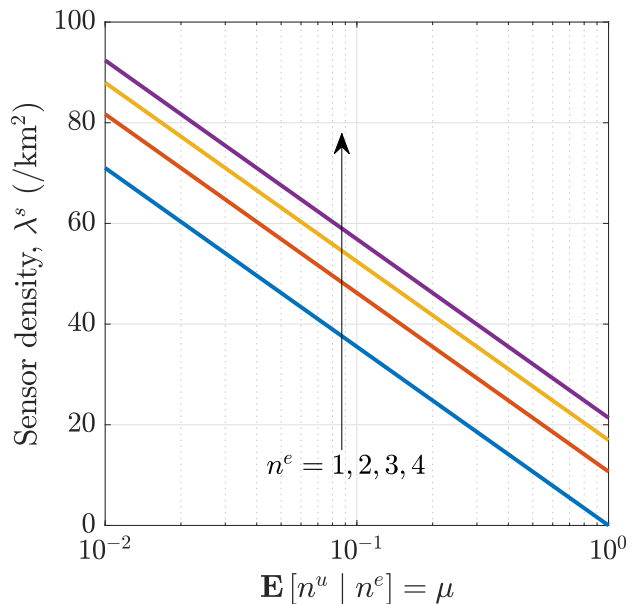


Fig. 9. A plot of (30) for $n^e = 1, 2, 3,$ and 4 . We use the parameters in Table II with omnidirectional sensors and emitters.

$\mathbb{E}[n^u | n^e] = \mu$ and solve for λ^s . For convenience, let $\Omega \triangleq \eta^e \eta^s \pi \mathbb{E}[h^\delta] (\omega / (\eta^e \eta^s))^\delta$. Solving for λ^s provides

$$\begin{aligned} \lambda^s &= \frac{1}{\Omega} \ln\left(\frac{n^e}{\mu}\right) \\ &= \frac{1}{\Omega \log_{10}(e)} [\log_{10}(n^e) - \log_{10}(\mu)]. \end{aligned} \quad (30)$$

For system design, if it is tolerable to miss an average of $\mathbb{E}[n^u | n^e] = \mu$, the corresponding sensor density could be found. As an example, Fig. 9 plots (30) for omnidirectional sensors and emitters with the parameters in Table II. We see that tolerating a larger average number of undetected emitters lowers the required sensor density. In Fig. 9, we see that increasing μ by an order of magnitude decreases the sensor density by about 35 sensors/km². Generally, this trade-off is given by $(\Omega \log_{10}(e))^{-1}$ per decade of μ .

V. CONCLUSION AND FUTURE WORK

Since the occurrence of directional emitters is inevitable in practice, we must account for directional emitters in the design of a spectrum monitoring system. Previous works on sensor networks offer insight into this design under the assumption of omnidirectional emitters but have not considered directional emitters. We presented a generalized framework to model a system of directional sensors and emitters, which can specialize to the omnidirectional case. With the framework, we found the probability that at least one sensor detects a single emitter in (20) and lower bound this probability for multiple emitters in (27). We also found the expected number of undetected emitters in (29). The analysis shows that omnidirectional sensors optimize these metrics. Furthermore, for a given probability of detection, the required sensor density has the relationship $\lambda^s \propto \left(\frac{1}{\Psi^e}\right)^{1-\delta}$, which means we need more sensors for emitters with higher directivity. One caveat for these conclusions is the case of free space propagation

($\alpha = 2$) for which azimuth directionality does not have an effect. Finally, the sensitivity of $\Pr(\mathcal{E})$ to frequency is analyzed in (23), and a strategy for multi-band deployment is developed from analysis of (24).

Additionally, the results help to design a sensor network to detect directional emitters by making explicit the trade-off between the sensor capabilities and deployment density. In particular, we show that for a fixed budget, one benefits from increasing the MDS (thereby lowering the cost of the sensor) in order to deploy a greater number of sensors. The increase in sensor quantity improves the probability of detection more than a lower MDS. In other words, sensor quantity is more important than sensor quality.

Future work should analyze the tightness of the bound in (27). Also, this work can be extended to the problem of localizing emitters, perhaps through the problem of unique sensor coverage [54] or through the problem of multiple coverage. Moreover, the framework in Sec. II extends to three dimensional sensor networks, and we can reconsider the problems in this paper in the more realistic three-dimensional case. Finally, the system model can be extended to a heterogeneous sensor network with individual sensor densities for each type of sensor.

REFERENCES

- [1] President's Council of Advisors on Science and Technology (PCAST), "Realizing the Full Potential of Government-Held Spectrum to Spur Economic Growth," Washington, D.C., Tech. Rep., 2012.
- [2] R. Berry, M. Honig, and R. Vohra, "Spectrum markets: Motivation, challenges, and implications," *IEEE Commun. Mag.*, vol. 48, no. 11, pp. 146–155, November 2010.
- [3] X. Wang, L. Kong, F. Kong, F. Qiu, M. Xia, S. Arnon, and G. Chen, "Millimeter wave communication: A comprehensive survey," *IEEE Commun. Surveys Tuts.*, vol. 20, no. 3, pp. 1616–1653, thirdquarter 2018.
- [4] M. G. Cotton and R. A. Dalke, "Spectrum Occupancy Measurements of the 3550–3650 Megahertz Maritime Radar Band Near San Diego, California," NTIA, Tech. Rep. TR-14-500, Jan. 2014.
- [5] R. Trautmann, "Handbook: Spectrum monitoring," International Telecommunication Union (ITU), Tech. Rep., 2011.
- [6] A. Chakraborty, M. S. Rahman, H. Gupta, and S. R. Das, "Specsense: Crowdsensing for efficient querying of spectrum occupancy," in *Proc. IEEE Conf. Comput. Commun. (INFOCOM)*, 2017.
- [7] M. M. Sohel, M. Yao, T. Yang, and J. H. Reed, "Spectrum access system for the citizen broadband radio service," *Computer*, vol. 53, no. 7, pp. 18–25, July 2015.
- [8] S. Bhattarai, J. J. Park, B. Gao, K. Bian, and W. Lehr, "An Overview of Dynamic Spectrum Sharing: Ongoing Initiatives, Challenges, and a Roadmap for Future Research," *IEEE Trans. on Cogn. Commun. Netw.*, vol. 2, no. 2, pp. 110–128, June 2016.
- [9] M. Palola, M. Höyhty, P. Aho, M. Mustonen, T. Kippola, M. Heikkilä, S. Yrjölä, V. Hartikainen, L. Tudose, A. Kivinen, R. Ekman, J. Hallio, J. Paavola, M. Mäkeläinen, and T. Hänninen, "Field trial of the 3.5 GHz citizens broadband radio service governed by a spectrum access system (SAS)," in *Proc. IEEE Int. Symp. Dynamic Spectrum Access Netw. (DySPAN)*, March 2017, pp. 1–9.
- [10] T. T. Nguyen, M. R. Souryal, A. Sahoo, and T. A. Hall, "3.5 GHz Environmental Sensing Capability Detection Thresholds and Deployment," *IEEE Trans. on Cogn. Commun. Netw.*, vol. 3, no. 3, pp. 437–449, Sept 2017.
- [11] A. Chakraborty, A. Bhattacharya, S. Kamal, S. R. Das, H. Gupta, and P. M. Djuric, "Spectrum patrolling with crowdsourced spectrum sensors," in *Proc. IEEE Conf. Comput. Commun. (INFOCOM)*, 2018.
- [12] T. Yucek and H. Arslan, "A survey of spectrum sensing algorithms for cognitive radio applications," *IEEE Commun. Surveys Tuts.*, vol. 11, no. 1, pp. 116–130, 1st Quart. 2009.
- [13] S. Haykin and P. Setoodeh, "Cognitive Radio Networks: The Spectrum Supply Chain Paradigm," *IEEE Trans. on Cogn. Commun. Netw.*, vol. 1, no. 1, pp. 3–28, March 2015.
- [14] Y. Zhao, L. Morales, J. Gaeddert, K. K. Bae, J. S. Um, and J. H. Reed, "Applying radio environment maps to cognitive wireless regional area networks," in *Proc. IEEE Int. Symp. Dynamic Spectrum Access Netw. (DySPAN)*, April 2007, pp. 115–118.
- [15] T. Taher, R. Attard, A. Riaz, D. Roberson, J. Taylor, K. Zdunek, J. Hallio, R. Ekman, J. Paavola, J. Suutala, J. Roning, M. Matinmikko, M. Höyhty, and A. MacKenzie, "Global spectrum observatory network setup and initial findings," in *Int. Conf. Cognitive Radio Oriented Wireless Netw. and Commun. (CROWNCOM)*, June 2014, pp. 79–88.
- [16] A. Nika, Z. Li, Y. Zhu, Y. Zhu, B. Zhao, X. Zhou, and H. Zheng, "Empirical validation of commodity spectrum monitoring," in *Proc. ACM Conf. Embedded Networked Sensor Syst. (SenSys)*. ACM, 2016.
- [17] S. Grönroos, K. Nybom, J. Björkqvist, J. Hallio, J. Auranen, and R. Ekman, "Distributed Spectrum Sensing Using Low Cost Hardware," *J. of Signal Process. Syst.*, vol. 83, no. 1, pp. 5–17, 2016.
- [18] B. V. den Bergh, D. Giustiniano, H. Cordobés, M. Fuchs, R. Calvo-Palomino, S. Pollin, S. Rajendran, and V. Lenders, "Electrosense: Crowdsourcing spectrum monitoring," in *Proc. IEEE Int. Symp. Dynamic Spectrum Access Netw. (DySPAN)*, March 2017, pp. 1–2.
- [19] M. Khaledi, M. Khaledi, S. Sarkar, S. Kasera, N. Patwari, K. Derr, and S. Ramirez, "Simultaneous power-based localization of transmitters for crowdsourced spectrum monitoring," in *Proc. ACM Int. Conf. on Mobile Computing and Netw. (MobiCom)*. New York, NY, USA: ACM, 2017, pp. 235–247.
- [20] N. Kleber, A. Termos, G. Martinez, J. Merritt, B. Hochwald, J. Chisum, A. Striegel, and J. N. Laneman, "Radiohound: A pervasive sensing platform for sub-6 GHz dynamic spectrum monitoring," in *Proc. IEEE Int. Symp. Dynamic Spectrum Access Netw. (DySPAN)*, March 2017, pp. 1–2.
- [21] M. G. Cotton. (2018, Nov.) Spectrum monitoring. ITS. [Online]. Available: <https://www.its.bldrdoc.gov/programs/spectrum-monitoring.aspx>
- [22] *CBRS Coexistence Technical Specifications*, CBRS-TS-2001, CBRS Alliance, Jul. 2020. [Online]. Available: <https://ongoalliance.org/wp-content/uploads/2021/04/CBRS-TS-2001-V3.1.0-Approved-for-publication.pdf>
- [23] *Test and Certification for Citizens Broadband Radio Service (CBRS)*, WINNF-TS-4004, Wireless Innovation Forum, Sep. 2020. [Online]. Available: <https://winnf.memberclicks.net/assets/CBRS/WINNF-TS-4004.pdf>
- [24] A. Goldsmith, *Wireless Communications*. Cambridge University Press, 2005.
- [25] M. A. Guvensan and A. G. Yavuz, "On coverage issues in directional sensor networks: A survey," *Ad Hoc Netw.*, vol. 9, no. 7, pp. 1238–1255, 2011.
- [26] E. Kranakis, D. Krizanc, and E. Williams, "Directional versus omnidirectional antennas for energy consumption and k-connectivity of networks of sensors," in *Principles of Distributed Syst.*, T. Higashino, Ed. Berlin: Springer, 2005, pp. 357–368.
- [27] S.-H. Kim and Y.-B. Ko, "A directional antenna based path optimization scheme for wireless ad hoc networks," *Mobile Ad-hoc and Sensor Netw.*, pp. 317–326, 2005.
- [28] A. Spyropoulos and C. S. Raghavendra, "Energy efficient communications in ad hoc networks using directional antennas," in *Proc. Annu. Joint Conf. IEEE Comput. and Commun. Soc.*, vol. 1, 2002, pp. 220–228.
- [29] L. Lazos and R. Poovendran, "Serloc: Secure range-independent localization for wireless sensor networks," in *Proc. ACM Workshop Wireless Security*. New York, NY, USA: ACM, 2004, pp. 21–30.
- [30] P. Brass, "Bounds on coverage and target detection capabilities for models of networks of mobile sensors," *ACM Trans. Sen. Netw.*, vol. 3, no. 2, Jun. 2007.
- [31] J. Ai and A. A. Abouzeid, "Coverage by directional sensors in randomly deployed wireless sensor networks," *J. Combinatorial Optimization*, vol. 11, no. 1, pp. 21–41, 2006.
- [32] M. Haenggi, *Stochastic Geometry for Wireless Networks*. Cambridge University Press, 2013.
- [33] C. K. Liang, C. H. Tsai, and T. H. Chu, "Coverage enhancing algorithms in directional sensor networks with rotatable sensors," in *Proc. IEEE Asia-Pacific Services Computing Conf. (APSCC)*, Dec 2011, pp. 377–383.
- [34] I. Bergel and Y. Noam, "Lower Bound on the Localization Error in Infinite Networks With Random Sensor Locations," *IEEE Trans. Signal Process.*, vol. 66, no. 5, pp. 1228–1241, 2018.
- [35] S. Aldalameh, M. Ghogho, and A. Swami, "Distributed detection of an unknown target in clustered wireless sensor networks," in *Proc. IEEE Workshop on Sig. Proc. Adv. in Wireless Comm. (SPAWC)*, 2011, pp. 126–130.

- [36] P. Zhang, I. Nevat, G. W. Peters, G. Xiao, and H.-P. Tan, "Event Detection in Wireless Sensor Networks in Random Spatial Sensors Deployments," *IEEE Trans. Signal Process.*, vol. 63, no. 22, pp. 6122–6135, 2015.
- [37] K. Pandey and A. Gupta, "On the Coverage Performance of Boolean-Poisson Cluster Models for Wireless Sensor Networks," in *Proc. IEEE Wireless Comm. and Networking Conf. (WCNC)*, 2020, pp. 1–6.
- [38] L. Kang, Y. Qi, W. Gao, A. Wang, and Z. Dong, "A Percolation Based Approach for Critical Density in Non-Orientation Directional Sensor Network," in *Int. Conf. Ubiquitous Comput. Commun. (IUCC) and Data Sci. Comput. Intell. (DSCI) and Smart Comput., Netw. Services (SmartCNS)*, 2019, pp. 89–94.
- [39] W. Meng and W. Xiao, "Energy-Based Acoustic Source Localization Methods: A Survey," *Sensors*, vol. 17(2), no. 376, pp. 1–20, 2017.
- [40] M. Petrova, P. Mähönen, and A. Osuna, "Multi-class classification of analog and digital signals in cognitive radios using support vector machines," in *Int. Symp. Wireless Commun. Systems (ISWCS)*, Sept 2010, pp. 986–990.
- [41] Z. Yang, Y.-D. Yao, S. Chen, H. He, and D. Zheng, "MAC protocol classification in a cognitive radio network," in *Annu. Wireless and Optical Commun. Conf. (WOCC)*, May 2010, pp. 1–5.
- [42] N. Shetty, S. Pollin, and P. Pawelczak, "Identifying Spectrum Usage by Unknown Systems using Experiments in Machine Learning," in *Proc. IEEE Wireless Comm. and Networking Conf. (WCNC)*, April 2009, pp. 1–6.
- [43] M. Bkassiny, Y. Li, and S. K. Jayaweera, "A survey on machine-learning techniques in cognitive radios," *IEEE Commun. Surveys Tuts.*, vol. 15, no. 3, pp. 1136–1159, 3rd Quart. 2013.
- [44] D. M. Pozar, *Microwave Engineering*, 4th ed. Wiley, 2012.
- [45] C. A. Balanis, *Antenna Theory: Analysis and Design*, 3rd ed. Wiley-Interscience, 2005.
- [46] V. Erceg, L. J. Greenstein, S. Y. Tjandra, S. R. Parkoff, A. Gupta, B. Kulic, A. A. Julius, and R. Bianchi, "An empirically based path loss model for wireless channels in suburban environments," *IEEE J. Sel. Areas Commun.*, vol. 17, no. 7, pp. 1205–1211, July 1999.
- [47] M. Bahrepour, N. Meratnia, and P. J. M. Havinga, "Sensor fusion-based event detection in wireless sensor networks," in *6th Ann. Int. Mobile and Ubiquitous Systems: Network. Services (MobiQuitous)*, 2009, pp. 1–8.
- [48] M. A. Al-Jarrah, A. Al-Dweik, M. Kalil, and S. S. Ikki, "Decision fusion in distributed cooperative wireless sensor networks," *IEEE Trans. Veh. Technol.*, vol. 68, no. 1, pp. 797–811, 2019.
- [49] J. Möller and F. P. Schoenberg, "Thinning spatial point processes into Poisson processes," *Advances in Applied Probability*, vol. 42, no. 2, pp. 347–358, 2010.
- [50] L. Fejes Tóth, *Lagerungen in der Ebene auf der Kugel und im Raum*. Springer, 1953.
- [51] X. Tang, X. Xu, and M. Haenggi, "Meta Distribution of the SIR in Moving Networks," *IEEE Trans. Commun.*, vol. 68, no. 6, pp. 3614–3626, 2020.
- [52] N. G. Kleber, "The Design of Widespread Spectrum Monitoring Systems," Ph.D. dissertation, Univ. of Notre Dame, 2021.
- [53] S. Rajendran, R. Calvo-Palomino, M. Fuchs, B. V. den Bergh, H. Corдобes, D. Giustiniano, S. Pollin, and V. Lenders, "Electrosense: Open and big spectrum data," *IEEE Commun. Mag.*, vol. 56, no. 1, pp. 210–217, Jan 2018.
- [54] M. Haenggi and A. Sarkar, "Unique coverage in Boolean models," *Stat. & Probability Lett.*, vol. 123, pp. 1–7, 2017.



Nikolaus Kleber (S'15-M'19) received the B.S., M.S., and Ph.D. degrees in Electrical Engineering from the University of Notre Dame, Notre Dame, IN, USA, in 2013, 2016, and 2021, respectively.

He joined Raytheon Technologies in 2019 and is currently a senior software engineer. His research interests include signal processing, interference-limited communications, and distributed spectrum monitoring.



Martin Haenggi (S'95-M'99-SM'04-F'14) received the Dipl.-Ing. (M.Sc.) and Dr.sc.techn. (Ph.D.) degrees in electrical engineering from the Swiss Federal Institute of Technology in Zurich (ETHZ) in 1995 and 1999, respectively. Currently he is the Freimann Professor of Electrical Engineering and a Concurrent Professor of Applied and Computational Mathematics and Statistics at the University of Notre Dame, Indiana, USA. In 2007–2008, he was a Visiting Professor at the University of California at San Diego, in 2014–2015 he was an Invited Professor at EPFL, Switzerland, and in 2021–2022 he is a Guest Professor at ETHZ.

He is a co-author of the monographs "Interference in Large Wireless Networks" (NOW Publishers, 2009) and "Stochastic Geometry Analysis of Cellular Networks" (Cambridge University Press, 2018) and the author of the textbook "Stochastic Geometry for Wireless Networks" (Cambridge, 2012) and the blog stogblog.net, and he published 18 single-author journal articles. His scientific interests lie in networking and wireless communications, with an emphasis on cellular, amorphous, ad hoc (including D2D and M2M), cognitive, vehicular, and wirelessly powered networks.

He served as an Associate Editor for the Elsevier Journal of Ad Hoc Networks, the IEEE Transactions on Mobile Computing (TMC), the ACM Transactions on Sensor Networks, as a Guest Editor for the IEEE Journal on Selected Areas in Communications, the IEEE Transactions on Vehicular Technology, and the EURASIP Journal on Wireless Communications and Networking, as a Steering Committee member of the TMC, and as the Chair of the Executive Editorial Committee of the IEEE Transactions on Wireless Communications (TWC). From 2017 to 2018, he was the Editor-in-Chief of the TWC. Currently he is an editor for MDPI Information. For both his M.Sc. and Ph.D. theses, he was awarded the ETH medal. He also received a CAREER award from the U.S. National Science Foundation in 2005 and three paper awards from the IEEE Communications Society, the 2010 Best Tutorial Paper award, the 2017 Stephen O. Rice Prize paper award, and the 2017 Best Survey paper award, and he is a Clarivate Analytics Highly Cited Researcher.



Jonathan D. Chisum (S'02–M'06–SM'17) received the Ph.D. in Electrical Engineering from the University of Colorado at Boulder in Boulder, Colorado USA, in 2011.

From 2012 to 2015 he was a Member of Technical Staff at the Massachusetts Institute of Technology Lincoln Laboratory in the Wideband Communications and Spectrum Operations groups. His work at Lincoln Laboratory focused on millimeter-wave phased arrays, antennas, and transceiver design for electronic warfare applications. In 2015 he joined the faculty of the University of Notre Dame where he is currently an Assistant Professor of Electrical Engineering. His research interests include millimeter-wave communications and spectrum sensing using novel and engineered materials and devices to dramatically lower the power and cost and enable pervasive deployments. His group focuses on gradient index (GRIN) lenses for low-power millimeter-wave beam-steering antennas, nonlinear (1-bit) radio architectures for highly efficient communications and sensing up through millimeter-waves, phase-change materials for reconfigurable RF circuits for wideband distributed circuits and antennas, and microwave/spin-wave structures for low-power and chip-scale analog signal processing for spectrum sensing and protection.

Dr. Chisum is a senior member of the IEEE, a member of the American Physical Society, and an elected Member of the U.S. National Committee (USNC) of the International Union of Radio Science's (URSI) Commission D (electronics and photonics). He is the past Secretary and current Vice-chair for USNC URSI Commission D: Electronics and Photonics.



Bertrand Hochwald (S'90–M'95–SM'06–F'08) was born in New York, NY, USA. He received the bachelor's degree from Swarthmore College, Swarthmore, PA, USA, the M.S. degree in electrical engineering from Duke University, Durham, NC, USA, and the M.A. degree in statistics, and the Ph.D. degree in electrical engineering from Yale University, New Haven, CT, USA.

From 1986 to 1989, he was with the Department of Defense, Fort Meade, MD, USA. He was a Research Associate and a Visiting Assistant Professor at the Coordinated Science Laboratory, University of Illinois at Urbana–Champaign, Urbana, IL, USA. In 1996, he joined the Mathematics of Communications Research Department, Bell Laboratories, Lucent Technologies, Murray Hill, NJ, USA, where he was a Distinguished Member of the Technical Staff. In 2005, he joined Beceem Communications, Santa Clara, CA, USA, as the Chief Scientist and Vice-President of Systems Engineering. He served as a Consulting Professor of Electrical Engineering at Stanford University, Palo Alto, CA, USA. In 2011, he joined the University of Notre Dame, Notre Dame, IN, USA, as a Freimann Professor of Electrical Engineering. Since 2018 he has been co-Director of the Wireless Institute.

Dr. Hochwald received several achievement awards while employed at the Department of Defense and the Prize Teaching Fellowship at Yale University. He has served as an Editor of several IEEE journals and has given plenary and invited talks on various aspects of signal processing and communications. He has forty-seven patents and has co-invented several well-known multiple-antenna techniques, including a differential method, linear dispersion codes, and multi-user vector perturbation methods. He received the 2006 Stephen O. Rice Prize for the best paper published in the IEEE Transactions on Communications. He co-authored a paper that won the 2016 Best Paper Award by a young author in the IEEE Transactions on Circuits and Systems. He also won the 2018 H. A. Wheeler Prize Paper Award from the IEEE Transactions on Antennas and Propagation. His PhD students have won various honors for their PhD research, including the 2018 Paul Baran Young Scholar Award from the Marconi Society. He is listed as a Thomson Reuters Most Influential Scientific Mind in multiple years. He was elected a Fellow of the National Academy of Inventors in 2019.



J. Nicholas Laneman (S'94–M'02–SM'07–F'14) is Director of SpectrumX – An NSF Spectrum Innovation Center, Founding Director and currently Co-Director of the Wireless Institute in the College of Engineering, and Professor in the Department of Electrical Engineering at the University of Notre Dame. He joined the faculty in August 2002 shortly after earning a Ph.D. in Electrical Engineering and Computer Science from the Massachusetts Institute of Technology (MIT). His research and teaching interests are in wireless system design, radio spectrum

access, technology standards and intellectual property, and regulatory policy. Laneman is an IEEE Fellow, has received the IEEE Kiyo Tomiyasu Award, the Presidential Early-Career Award for Scientists and Engineers (PECASE), and the NSF CAREER Award, and has been recognized twice by Thomson Reuters as an ISI Highly Cited Researcher. He is author or co-author on over 145 publications and is co-inventor on 8 U.S. patents.